A MATLAB-BASED APPROACH FOR ESTIMATING THE AREA TAKEN UP BY CELLS ATTACHED TO MICROPATTERNED OPTICALLY OPAQUE SURFACES

Yuri Dekhtyar, Hermanis Sorokins[#], and Sabīne Teifurova

Rīga Technical University, 6A Ķīpsalas Street, Rīga, LV-1048, LATVIA

[#] Corresponding author, hermanis.sorokins@rtu.lv

Contributed by Yuri Dekhtyar

Cell attachment is of paramount importance in implant design, bioreactor design, tissue engineering and the design of non-fouling surfaces. Surface roughness is a significant factor that affects cell attachment. To explore the impact of roughness characteristics, micromachining approaches can be used to fabricate surfaces with controlled microscale topography. When optical microscopy is employed to study cell attachment to optically opaque micropatterned surfaces, one needs to separate the area of an image coated with cells from the background. Manual cell counting can be used to assess the amount of attached cells. However, this process is very time consuming, when the studied surface is larger than several square millimeters. This paper describes an approach for the automatic estimation of the area of cells attached to the surfaces of micropatterned optically opaque platforms. Saccharomyces cerevisiae *yeast cells were used to test the developed approach. The approach uses image registration and segmentation tools available in MathWorks MATLAB R2020b Image Processing Toolbox. The factors that affect the accuracy of the developed approach (magnification, contrast and focus) as well as the ways of improving the results are discussed.*

Keywords: *cell attachment analysis, attached cell area, image processing, MATLAB, micropatterned surfaces.*

INTRODUCTION

Proper cell attachment to the surface of a substrate is a prerequisite in many biomedical and biotechnological applications (Tirrell *et al*., 2002; Li *et al*., 2017), for instance when designing implant surfaces (Bacakova *et al*., 2011) and scaffolds used for tissue engineering (Wu *et al*., 2014). One of the approaches for controlling cellular attachment to a substrate's surface is surface roughness engineering — the design of surfaces that either repel or entrap target cells, depending on the application (Nikkhah *et al*., 2012).

Micropatterning of surfaces to control cell attachment has found applications in the design of microfluidic devices (Ermis *et al*., 2018), bioreactors (Cui *et al*., 2011), anti-fouling materials (Cuello *et al*., 2020), tissue scaffolds (Chen *et al*., 2015) and implant surfaces (Pelaes-Vargas *et al*., 2011). The geometrical parameters of such surfaces — the shape,

height, length, width and the distance between microstructures — can be easily assigned using existing CAD software with the possibility of translating the developed models either into manufacturing documentation or for use in physical simulations. In coup with modern micromachining technologies (Gentili *et al*., 2005), these digital models can be used to manufacture cell immobilisation platforms that possess an array of surface roughness elements with strictly defined geometry. This in turn allows for the design of surfaces with the optimal parameters for the attachment and proliferation of target cells.

To understand which combination of surface roughness parameters will lead to the desired degree of cell attachment, optical microscopy studies of large substrate surfaces — millimetres to centimetres in area — should be prioritised over the random selection of only several fields of view to reduce statistical inconsistencies. However, when dealing

with such a large image set, the process of counting the attached cells for every field of view will be prohibitively time-consuming. Therefore, the use of automatic counting of attached cells is necessary. Techniques for cell counting on optically smooth surfaces are numerous and freely available (Cedena-Herrera *et al.*, 2015). Yet, when it comes to studying cell attachment to rough, optically opaque surfaces, considerable difficulties arise when trying to distinguish a cell from the surrounding substrate topography, thus prohibiting the use of simple contrast/brightness-based automatic cell counting techniques. In such cases fluorescent staining can improve the contrast between the cells and the surface; however, it cannot be used in cases when studying cell attachment since staining may disrupt a living cell's metabolism and alter its surface composition and with that its ability to attach to a substrate (Alford *et al*, 2009; Ansari *et al*, 2016). Therefore, an approach for counting the attached cells that can distinguish a cell from its surroundings without the use of fluorescence is required.

If the image of the surface roughness of a sample has been recorded before cell attachment occurred, then it can be filtered out from an image acquired after cell deposition was performed. Image registration algorithms make it possible to precisely overlay two similar images even if they were acquired with lateral or rotational shifts, if these shifts are not too large (Zitová *et al*, 2003). The use of cell immobilisation platforms with a strictly defined surface roughness that consists of an array of periodic elements as a surface for cell deposition makes image registration easier since (1) it requires only a single image of the surface taken before cell deposition to be used as an overlay (all surface regions that encompass several full microstructures are equivalent to every other region of the same size) and (2) similarities between the two surfaces become abundant due to the presence of recurring geometrical features, e.g., straight lines, which speeds up the process of convergence on the optimal overlay.

After overlaying the images, the intensity/colour contrast values of pixels for both images can be subtracted from one another and what is left can be considered as attached cells. Such a subtraction may lead to a resulting image with low contrast of the deposited cells vs. the background surface. To make the cells stand out an adaptive histogram equalisation algorithm can be used, which will stretch out the pixel intensity histogram, thus significantly increasing the range of pixel intensity values. Then, an image segmentation algorithm can be applied to separate out the now-visible cells from an evenly coloured background. This will allow to estimate the image area taken up by cells. All of the above-mentioned image processing tools are available in the MathWorks' MATLAB Image Processing Toolbox and can be combined into a single attached cell counting algorithm (MathWorks Nordic, 2020).

Thus, the aim of this work was to use the tools available in MathWorks' MATLAB for detection and estimation of the area taken up by unstained cells attached to a micropat-terned optically opaque surface. To accomplish this the following steps were performed:

1) design and fabrication of cell immobilisation platforms with an array of identical microscale structures that simulate surface roughness;

2) imaging of the surfaces of the immobilisation platforms before cells were deposited;

3) deposition of *Saccharomyces cerevisiae* (brewer's yeast) cells onto the surface of the immobilisation platforms from a liquid medium;

4) imaging of the surfaces of immobilisation platforms after cell deposition;

5) development of the approach for the detection and area estimation of attached cells;

6) validation of the developed approach.

MATERIALS AND METHODS

Cell immobilisation platform design and manufacturing. The immobilisation platforms were designed using SolidWorks 2018 (Dassault Systémes, Vélizy-Villacoublay, France). The parallelepiped was chosen as the repeating element of the microscale pattern that forms the platform's surface roughness. The elements within one pattern have the same height, lateral dimensions and spacing between structures along the X and Y axis. Two types of patterns — designated as Type 1 and Type 2 — with two different gap lengths between the sides of the structures were used for this study.

Based on these designs two sets of samples were manufactured at a semiconductor manufacturing facility (ALFA RPAR, Rīga, Latvia) using standard bulk micromachining approaches. The immobilisation platforms were manufactured on 470 micrometres thick (100) silicon wafers with a 0.6 μm layer of thermally grown silicon dioxide. The manufacturing process was as follows: the SiO_2 surface was covered with a layer of photoresist, then photolithography was performed using two different masks (one for each sample type), after which the exposed photoresist was removed through chemical etching. The exposed SiO_2 was removed by means of plasma-chemical etching, then the now-exposed layer of Si was removed by plasma etching forming parallelepiped-like structures. The remaining non-exposed photoresist was removed via chemical etching. Due to this process the 0.6 μm SiO_2 layer was left on the top of all microstructures forming a "plateau" with the rest of the sample being plain Si with a thin layer of natural oxide on top (< 10 nm).

The dimensions of the elements are given in Table 1 and images of the microscale pattern acquired using scanning electron microscopy (JSM-6400, JEOL, Japan) are given in Figure 1. The lateral dimensions of the immobilisation platforms were set at 5 × 5 mm^2.

110

Proc. Latvian Acad. Sci., Section B, Vol. **77** (2023), No. 2.

Table 1. Dimensions of immobilisation platform microscale pattern elements

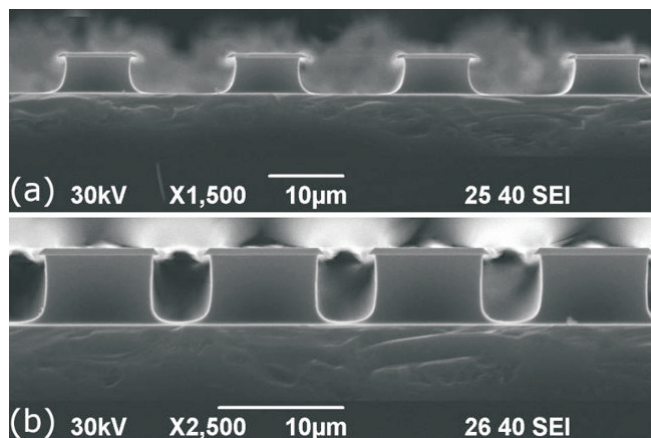| Sample type	Height, μm	Side length, μm	Gap length, μm	Density of structures per mm^2
Type 1	5.37 ± 0.14	10.4 ± 0.08	13.48 ± 0.12	1697
Type 2	6.19 ± 0.05	9.44 ± 0.08	4.49 ± 0.05	5041

Fig. 1. Scanning electron microscopy images of Type 1 (a) and Type 2 (b) structures taken from the side.

Cell deposition. Approximately 0.5 g of brewer's yeast (*S. cerevisiae*) were added to 150 ml of distilled water in a glass beaker and then mixed on a magnetic stirrer for two minutes or until the suspension became uniformly visually opaque. After that, a 1-ml sample of the suspension was taken to measure its optical absorbance at 600 nm with a Spectronic Helios Gamma UV-VIS spectrometer (ThermoFisher Scientific, USA). The suspension was repeatedly diluted until an optical absorbance value of 0.187 AU (absorbance units) has been reached. This particular absorbance value was chosen because at such low concentrations yeast cells tend to flocculate less, allowing to observe the attachment of both single cells and cell clusters.

Cell deposition was performed on four Type 1 samples and four Type 2 samples; eight samples were used in total. Deposition was performed simultaneously for all samples. The samples were placed into a dedicated socket on the outer ring of the sample holder, as described in (Baltacis *et al.*, 2020), located in a 90-mm Petri dish; then ~50 ml of suspension was added into the dish — enough to fully cover the sample surface with liquid when stationary and to stay suspended during rotation. The Petri dish was placed on an OS-20 orbital shaker (Biosan, Latvia) and rotated at 50 RPM for 60 minutes, after which the samples were kept stationary and in dispersion for 20 minutes. Then the liquid was slowly and carefully removed with a syringe and the samples were left to dry for five minutes. Then 50 ml of distilled water was added into the Petri dish, which was then once again rotated at 50 RPM for five minutes to wash away any non-attached cells. Lastly the water was removed with a syringe and the samples were placed into a thermostat for 15 minutes to dry at 30 °C.

Imaging of cells immobilised on the platforms. Sample imaging was performed using a NU-2 optical microscope (Carl Zeiss Jena, Germany) in reflected light mode at ×125 magnification. The microscope was equipped with an ocular-mounted digital camera (37MP HDMI, Eakins, China) and a custom-made motorised stage to enable movement along the XY-plane (perpendicular to the optical axis of the microscope) in increments of user-defined length (movement precision ±5 μm). The width and height of a single field of view (FOV) were 450 × 253 μm^2 (images acquired with a 16 : 9 aspect ratio). The surface of each sample was imaged sequentially starting at the top left corner in the XY plane of the sample and then progressing along the X-axis towards the top right corner of the sample and taking an image every 450 μm. After reaching the top right corner of the sample, the FOV was moved 253 μm along the Y-axis towards the bottom of the XY plane of the sample; then, an image was taken and then the movement progressed to the left-most part of the sample along the X-axis again in 450 μm increments. In this snake-like fashion the whole surface of each 5 × 5 mm^2 immobilisation platform was imaged, totalling 240 images per platform.

Development and implementation of an approach for attached cell analysis. Since the surface roughness of the immobilisation platforms is, in essence, an array of identical microscale structures, then the surface roughness image presented in a single FOV acquired from the surface of a clean immobilisation platform is equivalent to every other surface roughness image in a single FOV acquired from the surface of any other such immobilisation platform — with or without attached cells — given the magnification and lighting of the surfaces are the same for both FOVs and lateral/rotational discrepancies of the two FOVs are accounted for.

If two images are perfectly aligned, then one can subtract the pixel values of the clean immobilisation platform microscale structure FOV from the pixel values of the cell-deposited immobilisation platform FOV leaving differences in pixel intensities that correspond with the shape and location of deposited cells.

The remaining pixel intensities will be low — especially if cell/background contrast was poor — making their distribution on the intensity spectrum (for an 8-bit grayscale image this spectrum consists of 256 values with 0 being "black", 255 being "white" and everything in between being shades of "grey") skewed towards lower values. The intensity value distribution can be "stretched out" to fit the entirety of the available pixel intensity range using adaptive histogram equalisation, thus improving cell/background contrast.

This kind of image processing will make the cells distinct from the background, allowing for the use of automated segmentation algorithms, thus allowing to estimate the area taken up by cells attached to a micropatterned surface without the use of fluorescent staining.

Proc. Latvian Acad. Sci., Section B, Vol. **77** (2023), No. 2.

111

Firstly, images of immobilisation platform surfaces that did not undergo cell deposition, previously acquired using the same optical system parameters (magnification, light intensity, etc.), as were used when imaging platforms that did undergo cell deposition, were prepared to be used during the processing procedure. For convenience, these images were slightly rotated (up to 2 degrees in 0.1-degree increments) to position the sides of the structures in parallel to the edges of the images and cropped to remove any partially visible microscale structures that were present on the edges of the images.

The cropped images were used to make the "mask" images that would later be used during image processing. Two types of masks were made: (1) difference masks to be used as a fixed image during registration and as the image subtracted from the overlaid image of a platforms surface post deposition, and (2) binary masks image to be subtracted from the registered images so that separate estimation of the amount of cells attached on top and in between the microscale structures could be performed. The colour palate of the difference masks was the same as for the cropped image (8-bit Grayscale), while the binary masks were black-and-white images of the microscale structures, which were made by importing the cropped image into a vector graphics editor (Harrington *et al.*, 2020) and then creating an overlay of an array of black squares on a white background. The overlaid squares were of the same size as the tops of the surface microstructures. Examples of the two mask types made for Type 1 structures are given in Figure 2.

The image registration procedure starts with the definition of two grayscale images — one moving image and one fixed image. The moving image needs to be correctly superimposed on the fixed image to successfully perform the separation of the cell images from the background image. In this case, the post-deposition image was assigned as the moving image, while the difference mask image was assigned as the fixed image. Afterwards, the relationship between the intrinsic coordinates anchored to the rows (X direction) and columns (Y direction) of the structure images and the spatial location of the same row and column locations were stored in the internal world coordinate system as two objects that reference 2-D images to world coordinates, one for each image. Then the configurations for the multimodal intensity-based registration method were set up: the number of spatial samples was set to 500, the number of pixel intensity histogram bins was set to 70, all image pixels of a FOV were used, the growth factor of the search radius was set to 1.2, minimum size of the search radius was set to $1.5 \cdot 10^{-6}$, initial size of search radius was set to $8 \cdot 10^{-4}$, and the maximum number of iterations was set to 75. Next, the centres of the two objects were determined and translation coordinates for the moving image were calculated by subtracting the axis coordinates of the objects. An object that stores information about a 2-D affine geometric transformation using the postmultiply convention and enables forward and inverse transformations was initialised to store the translation coordinates to be used for coarse alignment in
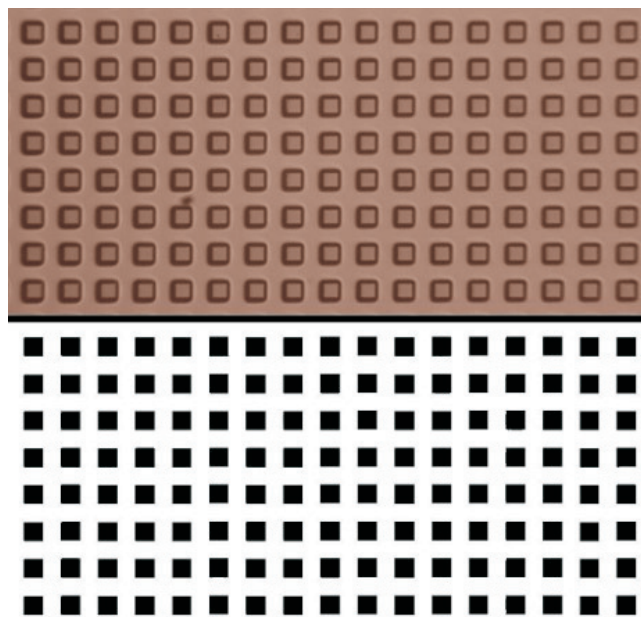

Fig. 2. Difference (top) and binary (bottom) mask images used during image processing of Type 1 immobilisation platform images.

the beginning of the image registration procedure. Gaussian blur was applied to the grayscale images to speed up the convergence of the registration procedure. The resulting images were initiated into new variables to be used as starter images with their intensity values normalised. Then the geometric transformation that aligns the moving image with the fixed image (i.e. the image registration procedure) was estimated using an automatic iterative intensity-based algorithm included with the MATLAB Image Processing Toolbox. After the registration procedure had converged on a satisfactory solution, the resulting translation/rotation coordinates were applied to the moving image. The new moving image was cropped to the size of the fixed mask image and saved for later use.

After image registration was performed, two composite images were made: the first composite image was the result of subtracting the binary mask from the difference mask and the second image was the result of subtracting the binary mask from the previously acquired registered image. The pixel intensity histograms of these two images underwent adaptive histogram equalisation and were also subtracted from each other. The resulting difference was saved as a grayscale image which depicted only the cells that became attached on top of the microscale structures of the immobilisation platform. A grayscale image that depicts only the cells that became attached between the microscale structures was acquired in a similar fashion by reversing the colours of the binary mask (the black squares are now white, and the areas in between are black).

Next, both images separately underwent segmentation using the Chan-Vese iterative region-growing image segmentation algorithm (Chan *et al.*, 2001) with the number of iterations set to 100. Before segmentation, however, the grayscale images were converted into a black and white image via

thresholding, then the holes in the structures observed in the image were filled, and then morphological opening of the resulting black-and-white image was performed with the morphological structuring element being a 3-by-3-pixel rectangle. The resulting segmented image was saved for later use and the procedure was repeated for the second image. Lastly, the number of segments that represent the attached cells and the area taken up by each of these segments for both images were calculated.

RESULTS

The developed approach (henceforth referred to simply as "algorithm") was applied to 40 images taken from Type 1 and Type 2 immobilisation platforms post cell deposition (20 images per type). As counted by the algorithm, the average fraction of the area taken up by cells in relation to the whole area of an FOV (average cell fraction) for Type 1 platforms was 1.46% ± 0.57%. For Type 2 platforms the average cell fraction was 0.99% ± 0.55%.

The algorithm underwent validation to check its accuracy in distinguishing cells from the background. This was accomplished by opening the images in an image editor and hand-marking the areas with attached cells, then calculating the area taken up by the hand-marked cells using MAT-LABs segmentation tool. Additionally, composite images that combine the original unmarked images of platform surfaces, images of cell-containing regions marked by the algorithm and images of cell-containing regions marked by hand were made for visual evaluation. Thus, both the veracity of the attached cell area values and the algorithm's cell detection sensitivity could be tested.

For each of the 40 images processed using the algorithm, hand-marking of cells was performed in GIMP 2.0 (GIMP Team) using the Pencil tool with a Hardness of 100 and a Size 5 Brush, which was equal to a spot of 21 pixels in area. These Pencil tool settings were used because the size of the resulting spot was similar in size and shape to an average yeast cell imaged with the settings used. Therefore, the area of the smallest possible cell area that contains only one cell was estimated to be 21 pixels. Marking was performed in a separate binary colour channel to exclude any bleed-over of pixel information from the base image into the new markup image. After finishing hand marking the areas taken up by cells, the markup image was exported as a new uncompressed 8-bit grayscale jpg image with the cell areas appearing as white shapes on a black background. Sample images depicting the sample's surface area and the cell areas marked by hand and by using the algorithm are given in Figure 3.

Then, all 40 hand-marked images were imported into MAT-LAB and segmented, the areas taken up by cells for each image being saved into a separate csv file. Total cell area values were calculated for each image and average cell fraction values were calculated for both platform types. For platforms of Type 1 the average cell fraction was 2.71 ±
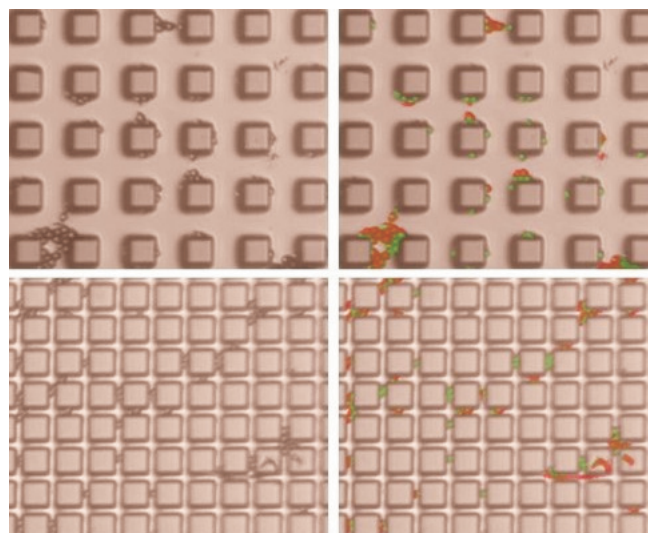

Fig. 3. Cropped FOVs of Type 1 (top) and Type 2 (bottom) immobilisation platform surfaces. Top right and bottom right images contain green and red overlays that correspond to markups made by hand and by the algorithm, respectively.
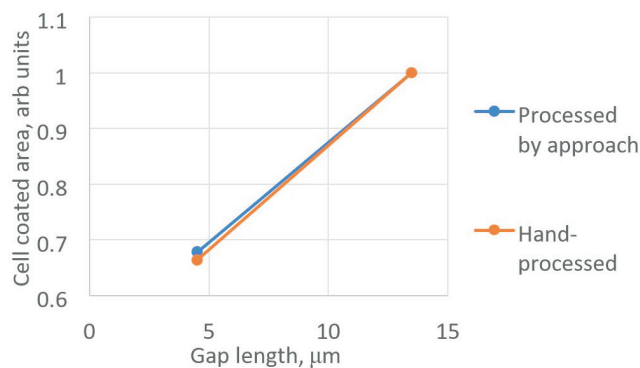

Fig. 4. Correlations of the effect of gap length on the cell coated area values estimated by using the approach vs. hand processing.

1.11% while for platforms of Type 2 the average cell fraction was 1.80% ± 0.89%. The average cell fraction values acquired through hand-marking were almost twice as large than those acquired by using the algorithm. In fact, the average error between hand-marked and algorithm-marked data for Type 1 platforms was 89% ± 42% and for Type 2 platforms it is 112% ± 97%. As shown in Figure 4, the error values for Type 1 platforms ranged from 22% to 180% for the difference between hand-marked and algorithm-marked data while for Type 2 platforms this difference ranges from 11% to 278%.

DISCUSSION

The results from the approach compared with hand marking were correspondingly 1.46 ± 0.57% against 2.71 ± 1.11% for the Type 1 platform and 0.99 ± 0.55% against 1.8 ± 0.89% for the Type 2 platform. The values of the area taken up by attached cells determined by the approach are lower than those gained from the manually processed data. Nevertheless, the arbitrary data demonstrate the same correlations, with the gap length as the most significantly varied factor (Fig. 4).

Proc. Latvian Acad. Sci., Section B, Vol. **77** (2023), No. 2.

113

Visual evaluation shows that the algorithm is capable of distinguishing clusters of cells from the background, but has limitations when distinguishing individual cells, specifically when cells are in close contact with the sides of the microstructures. Additionally, the algorithm underestimates the area of cell clusters. Difficulties when distinguishing cells from the background arise in areas of low contrast, where both the structures and the cells are similar in colour. Areas where the surface is under- or over-focused also remain under-marked or unmarked.

Since the algorithm is better at detecting cell clusters rather than single cells, statistical errors can occur. For example, if the image contains mostly single cells and only a few cell clusters and the algorithm detects and estimates the area taken up only by clusters, then this will lead to an underestimated value for the area of attached cells when compared to hand-marked images. If unmarked single cells are not present, the average error for Type 1 samples becomes reduced to 54.3% ± 33.2%.

Having fewer cell clusters per FOV also leads to statistical errors. As an example, the areas of a single cell (Fig. 5) acquired by using hand-marking and the algorithm differ by 88%. While the clusters appear similar in shape and size the numerical comparison of their areas shows an almost two-fold underestimation by the algorithm.

These inconsistencies are caused primarily by three kinds of errors, the first one being due to light scattering caused by the shape of the slope present on the sides of the microscale structures, which reduces the visibility of cells that are located close to the edges of the structures. This makes the use of intensity-based detection approaches challenging, as the cells may become partially or even fully indistinguishable from the background. The second error type occurs in cells that are farther away from the sides of the microscale structures, but are still partially in the structures' "shadow zone": during mask subtraction these cells lose the part that is occluded by the "shadow" and become morphologically open taking on the shape of a sickle instead of an ovoid. When during segmentation the resulting image undergoes closing, the cell does not return to its ovoid shape and only the sickle part is counted towards the total area of the cluster, thus reducing the overall area. The third type of error is caused by "overzealous" marking by the person responsible for hand-marking the images. In certain cases, cells that were poorly visible were marked based simply on the inference of the marker, leading to stark differences when comparing results acquired through algorithm-marking and hand-marking.

Magnification is another factor that may affect the sensitivity of the algorithm. Using magnifications higher than the ×125 used in this study might alleviate the effects of the previously mentioned errors. To check this assumption, test images of Type 1 and Type 2 immobilisation platforms were made before and after cell deposition using a ×20 objective for a total magnification of ×200. The acquired images were processed using the same approach as were the
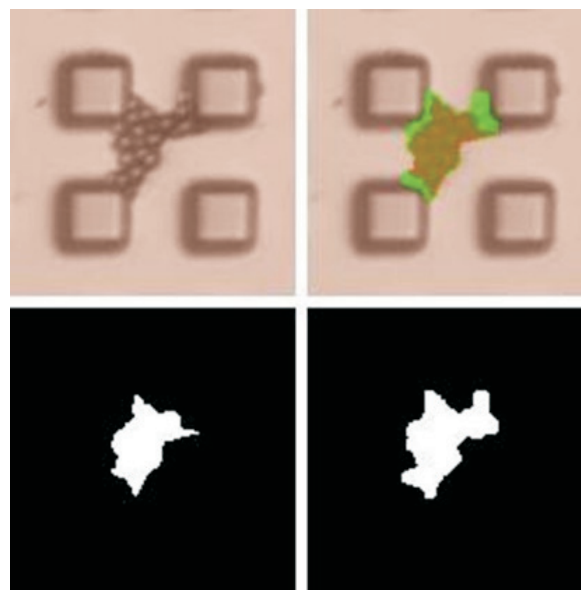

Fig. 5. A single cluster of cells. Top left image shows an unmarked cluster, top right image shows a cluster marked by hand (green) and by the developed algorithm (red), bottom left image shows a separate algorithm, bottom left image shows a separate algorithm-marked cluster while bottom right shows a separate hand-marked cluster.

ones acquired at ×125 magnification, the only difference being that new difference and binary masks that are applicable to the new magnification had to be made to accommodate the change in apparent microstructure dimensions. The resulting composite images can be seen in Figures 6 and 7. While the change in resulting error values was small — hand-marked vs. algorithm-marked areas differ by 40% and 71% for Type 1 and Type 2 immobilisation platforms, respectively — visual evaluation showed that with an increase in magnification single cells become visible and the outlines of marked clusters overlap more neatly than they would at a lower magnification. Errors caused by shadowing, cell morphological opening and over-zealous marking are still present.

CONCLUSIONS

An approach for estimating the area of cells attached to an optically opaque substrate with microscale surface roughness was developed using MathWorks' MATLAB R2020b. The developed approach uses image registration to overlay an image of a clean micropatterned surface over an image of an identical micropatterned surface with cells present on its surface. The background microscale structures are removed via image subtraction, and then the area taken up by the attached cells is determined via segmentation. The approach can be used to process images of cell immobilisation platforms with different types of microscale roughness acquired using a reflected light optical microscope with a magnification of ×125. The approach was validated by comparing its output to that gained from hand-marked images. The results from the approach compared with hand marking gave lower values of the cell coated areas. However, the correlations of the gap lengths with the cell coated
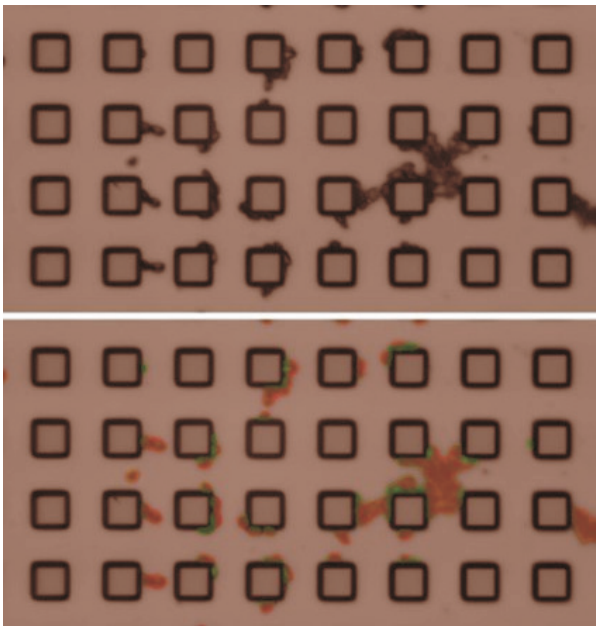
Fig. 6. At the top is an image of a Type 1 structure acquired with a magnification of ×200. At the bottom is a composite image that includes the microscale roughness, hand-marked (green) and algorithm-marked (red) cells.
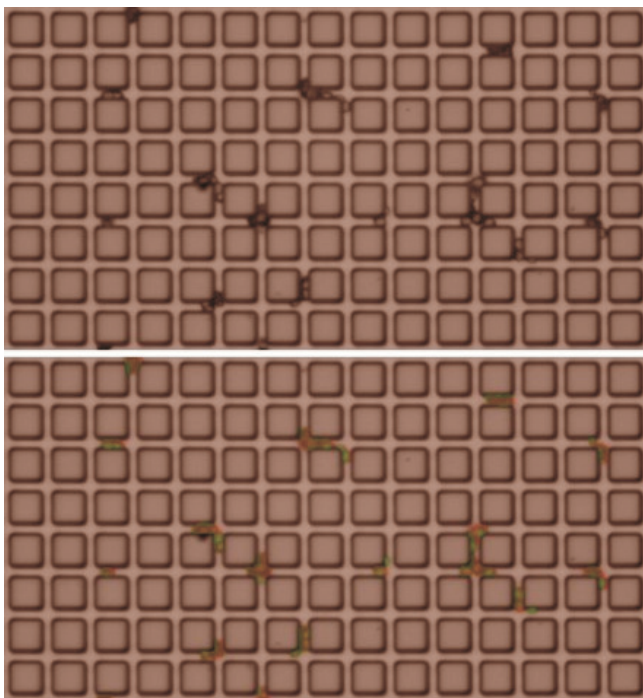

Fig. 7. At the top is an image of a Type 2 structure acquired with a magnification of ×200. At the bottom is a composite image that includes the microscale roughness, hand-marked (green) and algorithm-marked (red) cells.

area values estimated with the approach and hand processing were the same for the arbitrary units area scale.

Factors that may cause underestimation of the attached cell area by the developed approach include:

- Poor magnification — use of magnifications lower than ×200 may result in the algorithm missing individual cells.

- Poor cell/background contrast — may cause cells to become fully or partially hidden, especially if the cells are attached to the sides of microscale structures.

- Poor focus — may cause errors during image registration against the reference image as well as during cell marking.

The developed approach works best in cases when both images (with and without attached cells) are taken using identical lighting conditions and foci, when the contrast between the background surface roughness and the cells is sufficiently high, and when magnification is set to no less than ×200. The first condition improves image registration while the second and third conditions improve cell detection during segmentation.

ACKNOWLEDGEMENTS

REFERENCES

Alford, R., Simpson, H. M., Duberman, J., Hill, G. C., Ogawa, M., Regino, C., Kobayashi, H., Choyke, P. L. (2009). Toxicity of organic fluorophores used in molecular imaging: Literature review. *Mol. Imaging*, **8** (6), 7290.2009.00031. https://doi.org/10.2310/7290.2009.00031.

Ansari, A. M., Ahmed, A. K., Matsangos, A. E., Lay, F., Born, L. J., Marti, G., Harmon, J. W., Sun, Z. (2016). Cellular GFP toxicity and immunogenicity: Potential confounders in *in vivo* cell tracking experiments. *Stem Cell Rev. Rep.,* **12** (5), 553–559.
https://doi.org/10.1007/s12015-016-9670-8.

Bacakova, L., Filova, E., Parizek, M., Ruml, T., Svorcik, V. (2011). Modulation of cell adhesion, proliferation and differentiation on materials designed for body implants. *Biotechnol. Adv.*, **29** (6), 739–767.
https://doi.org/10.1016/j.biotechadv.2011.06.004.

Baltacis, K., Bystrov, V., Bystrova, A., Dekhtyar, Y., Freivalds, T., Raines, J., Rozenberga, K., Sorokins, H., Zeidaks, M. (2020). Physical fundamentals of biomaterials surface electrical Functionalization. *Materials*, **13** (20), 4575. https://doi.org/10.3390/ma13204575.

Cadena-Herrera, D., Esparza-De Lara, J. E., Ramírez-Ibañez, N. D., López-Morales, C. A., Pérez, N. O., Flores-Ortiz, L. F., Medina-Rivero, E. (2015). Validation of three viable-cell counting methods: Manual, semi-automated, and automated. *Biotechnol. Rep.*, **7**, 9–16.
https://doi.org/10.1016/j.btre.2015.04.004.

Chan, T. F., & Vese, L. A. (2001). Active contours without edges. IEEE Transactions on Image Processing, **10** (2), 266–277.
https://doi.org/10.1109/83.902291.

Chen, S., Nakamoto, T., Kawazoe, N., Chen, G. (2015). Engineering multi-layered skeletal muscle tissue by using 3D microgrooved collagen scaffolds. *Biomaterials*, **73**, 23.
https://doi.org/10.1016/j.biomaterials.2015.09.010.

Cuello, E. A., Mulko, L. E., Barbero, C. A., Acevedo, D. F., Yslas, E. I. (2020). Development of micropatterning polyimide films for enhanced antifouling and antibacterial properties. *Colloids Surf. B: Biointerfaces*, **188**, 110801. https://doi.org/10.1016/j.colsurfb.2020.110801.

Cui, Y., Huo, B., Sun, S., Yang, F., Gao, Y., Pan, J., Long, M. (2011). Fluid dynamics snalysis of a novel micropatterned cell bioreactor. *Ann. Biomed. Eng.*, **39** (5), 1592–1605. https://doi.org/10.1007/s10439-011-0250-4.

Proc. Latvian Acad. Sci., Section B, Vol. **77** (2023), No. 2.

115

Ermis, M., Antmen, E., Hasirci, V. (2018). Micro and nanofabrication methods to control cellsubstrate interactions and cell behavior: A review from the tissue engineering perspective. *Bioactive Mater.*, **3** (3), 355–369. https://doi.org/10.1016/j.bioactmat.2018.05.005

Gentili, E., Tabaglio, L., Aggogeri, F. (2005). Review on micromachining techniques. *AMST 05'. Adv. Manufact. Syst. Technol.*, **486**, 387–396. https://doi.org/10.1007/3-211-38053-1_37.

Harrington, B., Gould, T., Hurst, N., Inkscape's Contributors. (n.d.). Inkscape. Inkscape: Open Source Scalable Vector Graphics Editor. https://inkscape.org/ (accessed 22 November 2020).

Li, Y., Xiao, Y., Liu, C. (2017). The horizon of materiobiology: A perspective on material-guided cell behaviors and tissue engineering. *Chem. Rev.*, **117** (5), 4376–4421. https://doi.org/10.1021/acs.chemrev.6b00654.

MathWorks Nordic. Get Started with Image Processing Toolbox – MathWorks Nordic. (2020). https://se.mathworks.com/help/images/getting-startedhttps://se.mathworks.com/help/images/getting-started-with-image-processing-toolbox.htmlwith-image -processing-toolbox.html (accessed_22.11.2020).

Nikkhah, M., Edalat, F., Manoucheri, S., Khademhosseini, A. (2012). Engineering microscale topographies to control the cell–substrate interface. *Biomaterials*, **33** (21), 5230–5246. https://doi.org/10.1016/j.biomaterials.2012.03.079.

Pelaez-Vargas, A., Gallego-Perez, D., Magallanes-Perdomo, M., Fernandes, M. H., Hansford, D. J., De Aza, A. H., Pena, P., Monteiro, F. J. (2011). Isotropic micropatterned silica coatings on zirconia induce guided cell growth for dental implants. *Dental Mater.*, **27** (6), 581–589. https://doi.org/10.1016/j.dental.2011.02.014.

Tirrell, M., Kokkoli, E., Biesalski, M. (2002). The role of surface science in bioengineered materials. *Surf. Sci.*, **500** (1–3), 61–83. https://doi.org/10.1016/s0039-6028(01)01548-5.

Wu, S., Liu, X., Yeung, K. W. K., Liu, C., Yang, X. (2014). Biomimetic porous scaffolds for bone tissue engineering. *Mater. Sci. Eng.*, **80**, 1–36. https://doi.org/10.1016/j.mser.2014.04.001.

Zitová, B., Flusser, J. (2003). Image registration methods: A survey. *Image Vision Comput.*, **21** (11), 977–1000. https://doi.org/10.1016/s0262-8856(03)00137-9.

UZ MATLAB RĪKIEM BALSTĪTĀ PIEEJA PIE OPTISKI NECAURSPĪDĪGĀM MIKROSTRUKTURĒTĀM VIRSMĀM PIESTIPRINĀTU ŠŪNU LAUKUMA IZVĒRTĒŠANAI

Šūnu piesaistei ir ārkārtīgi liela nozīme implantu, bioreaktoru un šūnas un molekulas nepiesaistošo virsmu izstrādē, kā arī audu inženierijā. Virsmas raupjums ir būtisks faktors, kas ietekmē šūnu pieķeršanos pie virsmas. Lai izpētītu raupjuma specifikas ietekmi uz šūnu piesaisti, var izmantot virsmas mikromehāniskās apstrādes pieejas, lai izgatavotu virsmas ar kontrolētu mikromēroga topogrāfiju. Pētot šūnu piesaisti pie optiski necaurspīdīgām mikrostrukturētām virsmām, izmantojot optisko mikroskopiju, piesaistīto šūnu laukums ir jāatdala no raupjuma, kas tam ir fonā. Lai novērtētu pievienoto šūnu daudzumu, var izmantot šūnu manuālu skaitīšanu, taču šis process ir ļoti laikietilpīgs, ja pētāmā virsma ir lielāka par vairākiem kvadrātmilimetriem. Šajā rakstā aprakstīta pieeja, kura dod iespēju automātiski novērtēt laukumu šūnām, kuras piestiprinātas pie mikrostrukturētām optiski necaurspīdīgu platformu virsmām. Lai pārbaudītu izstrādāto pieeju, tika izmantotas *S. cerevisiae* rauga šūnas. Šī pieeja izmanto attēlu reģistrācijas un segmentācijas rīkus, kas pieejami *MathWorks MATLAB R2020b Image Processing Toolbox*. Tiek apspriesti faktori, kas ietekmē izstrādātās pieejas precizitāti (palielinājums, kontrasts un fokuss), kā arī rezultātu uzlabošanas veidi.